

NLO QCD predictions for doubly-polarized WZ production at the LHC

Ansgar Denner^a, Giovanni Pelliccioli^a

^aUniversity of Würzburg, Institut für Theoretische Physik und Astrophysik, Emil-Hilb-Weg 22, 97074 Würzburg (Germany)

Abstract

Accessing the polarization of weak bosons provides an important probe for the mechanism of electroweak symmetry breaking. Relying on the double-pole approximation and on the separation of polarizations at the amplitude level, we study WZ production at the LHC, with both bosons in a definite polarization mode, including NLO QCD effects. We compare results obtained defining the polarization vectors in two different frames. Integrated and differential cross-sections in a realistic fiducial region are presented.

Keywords: Di-boson, LHC, Polarization, Electroweak, NLO QCD

1. Introduction

The investigation of di-boson production represents a crucial target for the Large Hadron Collider (LHC) with the accumulated Run 2 data. These processes provide a direct probe of the non-abelian character of electroweak interactions in the Standard Model (SM) as well as of possible deviations from standard triple-gauge-boson-coupling interactions due to new physics. On top of this, the study of the weak-boson polarization supplies a probe of the mechanism of electroweak symmetry breaking, which is responsible for the appearance of a longitudinal polarization mode of massive gauge bosons.

Among di-boson processes, $W^\pm Z$ production with fully-leptonic decays is optimal to extract detailed information on polarizations, as it features a sizeable rate at the LHC (higher than ZZ, smaller than W^+W^-) and gives almost complete access to the final-state kinematics, up to the reconstruction of the single neutrino (impossible in fully-leptonic W^+W^-).

The CMS and ATLAS collaborations have measured the inclusive and differential production of $W^\pm Z$ at the LHC at 13 TeV centre-of-mass (CM) energy [1–3], and recently ATLAS has also measured polarization fractions for the W and the Z boson in this process [4]. In the experimental community there is increasing interest in the measurement of the polarization of single bosons produced in electroweak processes, as well as in the extraction of signals with two polarized bosons, in processes like inclusive di-boson production and vector-boson scattering.

The WZ hadronic production in the SM has been intensely investigated in the theoretical community. The next-to-leading-order (NLO) QCD corrections are known since many years [5, 6]. NLO electroweak (EW) corrections have been calculated for the on-shell [7, 8] and the off-shell case [9]. Next-to-next-to-leading-order (NNLO) QCD corrections are known

in the on-shell case [10], including off-shell effects [11] and combined with EW corrections [12]. Beyond fixed order, computations including resummed predictions [13] and matching to parton shower [14, 15] are also available. WZ production is also relevant for the study of anomalous triple-gauge-boson couplings [16–19].

Weak-boson polarizations in WZ production at the LHC have been first investigated in Ref. [20] at leading order (LO). NLO QCD and EW effects on fiducial polarization observables have been studied in Refs. [21, 22] in the case where only one of the two bosons has a definite polarization state. The automated Monte Carlo simulation of boson-pair production with polarized weak bosons is currently well-established in MADGRAPH 5 [23] in the narrow-width approximation (NWA), but the perturbative accuracy is limited to LO. Since the measurement of WZ production with both bosons in a definite polarization mode (which we call *doubly-polarized* for simplicity) represents a major aim for experimental collaborations, an improved theoretical description of these polarized signals is definitely needed to compare with data.

The work presented in this paper, using the methods introduced in Ref. [24], improves the perturbative accuracy for doubly-polarized WZ production at the LHC, including NLO QCD effects, and enables a precise modelling of off-shell effects and interferences among polarized amplitudes.

Furthermore, recent experimental results [4, 25] and theoretical studies [22, 26] in di-boson and vector-boson scattering have addressed a novel definition of polarizations in the *modified helicity coordinate system*. In this definition, the reference axis is fixed by the direction of the corresponding boson in the di-boson CM frame, and not in the laboratory frame (*helicity coordinate system* [27]). We present in this paper results for both polarization definitions, analysing the main differences under a theoretical perspective and keeping in mind the limited sensitivity of the LHC to polarized signals. Even though some results for singly-polarized cross-sections are shown, the main focus of this paper is put on doubly-polarized predictions.

The paper is organized as follows. In Sect. 2 we briefly recall

Email addresses: ansgar.denner@physik.uni-wuerzburg.de
(Ansgar Denner), giovanni.pelliccioli@physik.uni-wuerzburg.de
(Giovanni Pelliccioli)

the methods employed to define a polarized signal at the amplitude level. We also detail the SM parameters and selection cuts that we have used in Monte Carlo simulations. In Sect. 3 we show numerical results for polarized signals with both definitions of polarizations. Our conclusions are given in Sect. 4.

2. Details of the calculation

2.1. Polarized signal definition

In order to define singly- and doubly-polarized signals in WZ production, we apply the technique detailed in Ref. [24], which relies on the double-pole approximation (DPA) [28–33] for the gauge-invariant treatment of resonant diagrams, and on the separation of polarizations in weak-boson propagators at the amplitude level [34]. This technique has been applied also to real-radiation squared amplitudes and to subtraction counterterms that contribute to the NLO QCD cross-sections. This ensures that a specific polarization mode for one or both bosons is coherently selected in all parts of the calculation. Such a strategy allows us to define polarized signals in a natural manner, enabling the modelling of off-shell effects and spin correlations. Moreover, it is expected to be more accurate than methods that rely either on the NWA or on a reweighting procedure [35]. Furthermore, defining polarizations at the amplitude level enables to account for the correlation between the two weak bosons, which are very important in di-boson production [24].

One purpose of this paper is to investigate different polarization definitions. It is well known that the polarization vectors for a weak boson need to be defined in a specific reference frame. In di-boson production, natural frames are the laboratory (LAB) and the di-boson centre-of-mass (CM) frame. In the definition of Ref. [27], the reference axis for polarization vectors of a single boson is fixed by its direction in the LAB reference frame. In the one of Ref. [4], the reference axis is the corresponding direction in the di-boson CM frame. Results in the two definitions cannot be easily related to each other as the two reference frames are connected by non-trivial Lorentz transformations. However, a comparison is useful to extract information about the spin structure of the process, as well as to highlight relevant observables which maximize the discrimination power among polarization states.

In the following, two polarization modes are considered for weak bosons: longitudinal (L) and transverse (T). The transverse one is understood as the coherent sum of the left- and right-handed modes. This choice results in four doubly-polarized signals: $W_L Z_L$, $W_L Z_T$, $W_T Z_L$, $W_T Z_T$. Singly-polarized signals for the W(Z) boson are labelled as $W_\lambda Z_U$ ($W_U Z_\lambda$), where $\lambda = L, T$, and U stands for unpolarized.

As in Ref. [24], the polarized and unpolarized tree-level and one-loop amplitudes are provided by RECOLA [36, 37] and COLLIER [38, 39]. The numerical integration is performed with the MoCANLO Monte Carlo code, which embeds Catani–Seymour dipoles [40] for the subtraction of infrared singularities, and is interfaced with parton distribution functions (PDFs) via LHAPDF6 [41].

2.2. Setup(s)

We consider the process $pp \rightarrow e^+ \nu_e \mu^+ \mu^- + X$ at 13 TeV CM energy. At tree-level [$\mathcal{O}(\alpha^4)$], such a process receives contributions only from the $q\bar{q}$ partonic channel, while the inclusion of QCD radiative corrections [$\mathcal{O}(\alpha_s \alpha^4)$] enables real contributions from the $qg(\bar{q}g)$ initial state.

Following Ref. [42], the weak-boson on-shell masses and widths are chosen as

$$\begin{aligned} M_W^{\text{os}} &= 80.379 \text{ GeV}, & \Gamma_W^{\text{os}} &= 2.085 \text{ GeV}, \\ M_Z^{\text{os}} &= 91.1876 \text{ GeV}, & \Gamma_Z^{\text{os}} &= 2.4952 \text{ GeV}, \end{aligned} \quad (1)$$

and then converted into the corresponding pole masses [43] which serve as inputs for the Monte Carlo simulations. The electroweak coupling is fixed in the G_μ scheme, with

$$G_\mu = 1.16638 \cdot 10^{-5} \text{ GeV}^{-2}. \quad (2)$$

The Higgs-boson and top-quark parameters do not enter the computation at the considered accuracy. Unstable bosons and weak couplings are treated in the complex-mass scheme [31, 44, 45]. We employ NNPDF3.1 parton distribution functions [46], computed with $\alpha_s(M_Z) = 0.118$ at LO and NLO for the LO and NLO QCD predictions, respectively. The renormalization and factorization scales are simultaneously set to $\mu_F = \mu_R = (M_Z + M_W)/2$ (pole masses).

To validate polarized calculations, we have studied an *inclusive setup*, which only includes a cut on the $\mu^+ \mu^-$ invariant mass that is constrained to be close to the Z mass,

$$81 \text{ GeV} < M_{\mu^+ \mu^-} < 101 \text{ GeV}. \quad (3)$$

Then, we have considered a *fiducial setup* that mimics the signal region of Ref. [4]. The following selections are applied:

- a minimum transverse momentum cut for the positron, $p_{T,e^+} > 20 \text{ GeV}$, and for the (anti)muon, $p_{T,\mu^\pm} > 15 \text{ GeV}$;
- a maximum rapidity cut for all charged leptons, $|y_\ell| < 2.5$;
- a minimum rapidity–azimuthal-angle distance cut for lepton pairs, $\Delta R_{\mu^+ \mu^-} > 0.2$ and $\Delta R_{\mu^\pm e^\pm} > 0.3$;
- a lower cut on the W-boson transverse mass,

$$M_{T,W} = \sqrt{2 p_{T,e^+} p_{T,\nu_e} (1 - \cos \Delta\phi_{e^+ \nu_e})} > 30 \text{ GeV}. \quad (4)$$

- the cut specified in Eq. (3).

No veto is imposed on the hadronic jets that may originate from real radiation at NLO QCD.

We have only considered the case of two unequal-flavour pairs of leptons. Performing an analogous study for same-flavour leptons would not introduce further conceptual issues in the signal definition. In fact, we expect that the presence of identical leptons would not lead to large interference effects. Furthermore, the additional ambiguity in identifying the candidate leptons reconstructing the Z and the W boson can be treated by proper selection cuts.

All of the presented results concern the production of a $W^+ Z$ in the *fiducial setup*. The charge-conjugate process can be studied analogously.

	σ_{LO} [fb]	fraction _{LO}	σ_{NLO} [fb]	fraction _{NLO}	K -factor
full	19.537(7) ^{+4.1%} _{-4.9%}	-	35.27(1) ^{+5.2%} _{-4.2%}	-	1.81
unpolarized (DPA)	19.125(6) ^{+4.1%} _{-5.0%}	100%	34.63(1) ^{+5.3%} _{-4.2%}	100%	1.81
polarizations defined in the CM frame					
$W_L^+Z_U$ (DPA)	3.502(1) ^{+4.8%} _{-5.7%}	18.3%	7.308(2) ^{+6.1%} _{-4.9%}	21.1%	2.09
$W_T^+Z_U$ (DPA)	15.480(6) ^{+4.0%} _{-4.8%}	80.9%	27.14(1) ^{+5.0%} _{-4.1%}	78.4%	1.75
$W_U^+Z_L$ (DPA)	3.451(1) ^{+4.8%} _{-5.7%}	18.0%	7.137(2) ^{+6.0%} _{-4.9%}	20.6%	2.07
$W_U^+Z_T$ (DPA)	15.674(6) ^{+4.0%} _{-4.8%}	81.9%	27.449(9) ^{+5.0%} _{-4.1%}	79.2%	1.75
$W_L^+Z_L$ (DPA)	1.508(1) ^{+4.5%} _{-5.3%}	7.9%	1.968(1) ^{+2.7%} _{-2.2%}	5.7%	1.31
$W_L^+Z_T$ (DPA)	2.018(1) ^{+5.1%} _{-6.0%}	10.6%	5.354(1) ^{+7.3%} _{-5.9%}	15.5%	2.65
$W_T^+Z_L$ (DPA)	1.902(1) ^{+5.0%} _{-5.9%}	9.9%	5.097(2) ^{+7.4%} _{-5.9%}	14.7%	2.68
$W_T^+Z_T$ (DPA)	13.555(5) ^{+3.8%} _{-4.7%}	70.9%	21.992(9) ^{+4.5%} _{-3.6%}	63.5%	1.62
polarizations defined in the LAB frame					
$W_L^+Z_U$ (DPA)	4.227(1) ^{+4.8%} _{-5.7%}	22.1%	8.160(2) ^{+5.6%} _{-4.6%}	23.6%	1.93
$W_T^+Z_U$ (DPA)	14.865(5) ^{+3.9%} _{-4.8%}	77.7%	26.394(9) ^{+5.1%} _{-4.1%}	76.2%	1.78
$W_U^+Z_L$ (DPA)	5.528(2) ^{+4.7%} _{-5.6%}	28.9%	9.550(4) ^{+4.9%} _{-4.0%}	27.6%	1.73
$W_U^+Z_T$ (DPA)	13.654(5) ^{+3.9%} _{-4.8%}	71.4%	25.052(8) ^{+5.3%} _{-4.3%}	72.3%	1.83
$W_L^+Z_L$ (DPA)	1.0824(4) ^{+4.1%} _{-4.9%}	5.7%	2.063(1) ^{+5.6%} _{-4.5%}	6.0%	1.91
$W_L^+Z_T$ (DPA)	3.165(1) ^{+5.1%} _{-6.0%}	16.5%	6.108(2) ^{+5.6%} _{-4.5%}	17.6%	1.93
$W_T^+Z_L$ (DPA)	4.381(2) ^{+4.8%} _{-5.7%}	22.9%	7.409(4) ^{+4.8%} _{-3.8%}	21.4%	1.69
$W_T^+Z_T$ (DPA)	10.526(4) ^{+3.6%} _{-4.4%}	55.0%	18.964(7) ^{+5.2%} _{-4.2%}	54.8%	1.80

Table 1: Integrated cross-sections (in fb) in the fiducial setup for unpolarized, singly-polarized and doubly-polarized W^+Z production. Polarizations are defined in the CM and the LAB frames. Numerical errors (in parentheses) and uncertainties from 7-point scale variations (in percentage) are shown. The fractions (in percentage) are computed as ratios of polarized cross-sections over the DPA unpolarized one. K -factors are computed as ratios of the NLO QCD over the LO cross-sections.

3. Results

We have thoroughly validated our calculation in the inclusive setup introduced in Sect. 2.2. In the absence of cuts on the leptons, interferences among polarization states vanish for most of the relevant variables, and polarized signals can be extracted by suitable projections on the unpolarized distributions in the decay angles [20, 34]. The comparison of Monte Carlo results for polarized cross-sections with those projected out of the unpolarized distributions has given perfect agreement both for polarization fractions and in the shapes of decay-angle distributions ($< 0.5\%$ discrepancy at both integrated and differential level). This holds for singly-polarized signals, but also for doubly-polarized results that can be analogously extracted from the singly-polarized ones. The validation has been done both for polarizations defined in the CM and in the LAB frames.

As a further check, we have compared LO integrated polarized results in the CM definition with those obtained with MADGRAPH 5 [23], finding good agreement ($\lesssim 1\%$ level).

In the following we present selected integrated and differential results for the fiducial setup described in Sect. 2.2.

3.1. Integrated cross-sections

Very large K -factors characterize the production of WZ at high-energy hadron collisions. The large QCD corrections are related to the approximate radiation-zero at Born level [47], which suppresses the LO prediction but is not present in the real corrections at NLO QCD [10].

In Table 1 we show integrated cross-sections in the fiducial region for unpolarized and polarized bosons. The full process is considered as a reference, as it includes all resonant and non-resonant effects. The unpolarized process in DPA is regarded as the unpolarized di-boson signal. The difference between the full and the DPA unpolarized results is considered as a background to di-boson production [24], and amounts to 2.1% (1.8%) at LO (NLO) QCD at the integrated level.

Summing singly- or doubly-polarized cross-sections and comparing the result against the DPA unpolarized result, one can extract information about the interferences among polarization states. Surprisingly, these effects never exceed 0.8% in absolute value, with both the LAB and the CM definition, despite the application of lepton cuts which, in general, are expected to generate non-vanishing interferences [20, 48].

The cross-sections for a polarized W^+ and an unpolarized Z boson show similar behaviours in the two definitions: the longitudinal K -factor is about 2, the longitudinal fraction is roughly 21% in the CM definition, not so far from the 24% in the LAB definition. A slightly different situation is found for a polarized Z boson produced with an unpolarized W , likely due to the asymmetric cuts on the leptons: the longitudinal fraction in the LAB definition (28%) is higher than in the CM one (21%), despite a larger impact of QCD corrections in the CM one. For singly-polarized results in both definitions, the fractions are only mildly sensitive to the inclusion of QCD corrections.

The differences between the CM and the LAB definitions of polarizations are much more evident when considering doubly-polarized cross-sections. The polarization fractions in the LAB definition are roughly conserved when going from LO to NLO QCD, as already found in W^+W^- production [24], while this is not the case in the CM definition. Furthermore, very different K -factors emerge in the two definitions: in the CM one both mixed polarization states feature a +170% enhancement due to QCD corrections, while in the LAB one the LT and TL polarization states are enhanced by 90% and 70%, respectively. The LL polarization mode defined in the CM frame features a very small K -factor (1.31), which is surprising given the larger QCD corrections in the singly-longitudinal cases. On the contrary, the same mode in the LAB definition features a +90% enhancement due to QCD corrections. At NLO QCD, the LL signal amounts to roughly 6% of the total in both definitions. The TT signal is larger in the CM definition, and conversely the mixed contributions are larger in the LAB one.

The back-to-back kinematics of the bosons in the CM frame at LO implies that the polarization vectors of the two weak bosons are defined with respect to the same reference axis, up to a change of sign. This leads to very similar results for the LT and TL polarization modes defined in the CM frame, despite the differences in the boson–lepton coupling between the W and the Z boson. This is not the case in the LAB-frame definition. The LL mode defined in the di-boson CM frame is singled out by the fact that both polarization vectors only depend on the di-boson momentum and on the momentum of a single boson. On the contrary, the longitudinal polarization vectors defined in the LAB frame depend on more physical quantities, resulting in a more involved spin structure. This qualitative argument indicates that the CM definition of polarization is more natural than the LAB one for di-boson processes.

A due comment is related to correlations. The wrong assumption that the spins of the two weak bosons are not correlated would lead to results which can be far from the correct ones. When defining polarizations in the CM frame, multiplying the two NLO singly-longitudinal fractions, one obtains 4.3%, which is substantially different from the predicted LL fraction (5.7%). The difference is larger at LO, where the kinematic is more constrained due to the absence of additional QCD radiation: the zero-spin-correlation assumption gives 3.3% for the LL fraction, whose actual value is 7.9%. In the LAB definition, these correlations are smaller: at (N)LO the combination of the two singly-longitudinal fractions gives 6.4% (6.5%),

which is not so far from the Monte Carlo result for the LL fraction, namely 5.7% (6%). The correlations are milder for the mixed states and very small for the TT state, both in the CM and in the LAB definition.

The rationale is that, in order to correctly model doubly-polarized signals, all spin-correlations must be properly accounted for. Separating polarizations at the amplitude level furnishes the safest and most natural strategy in this sense.

3.2. Distributions

We start this section commenting on the non-resonant background. At the integrated level, the impact of off-shell effects amounts to 2%, and this is also the case in most of the differential distributions accessible at the LHC. A larger non-resonant background is found in some suppressed phase-space regions, where non-resonant diagrams give a sizeable contribution, and therefore the DPA cannot reproduce accurately the full calculation. Large effects concern the tails of the distributions for the missing transverse momentum (10% at 500 GeV), the invariant mass of the four leptons (20% at 1.5 TeV), and the positron transverse momentum (15% at 500 GeV). The largest non-resonant background is found in the kinematic region where the transverse mass of the $e^+\nu_e$ pair is larger than the W -boson mass (30% at 100 GeV, 70% at 150 GeV). However, given the limited statistics of Run 2 data, these regions will be hardly accessible and therefore not really relevant for the analyses.

Also interferences among polarizations at the differential level reflect the integrated results in most of the phase-space regions. Their size never exceeds 2–3% in all relevant rapidity, transverse-momentum and angular distributions of the final-state particles.

In Figures 1–5 we show the differential distributions in five significant kinematic variables, for both the unpolarized and doubly-polarized process. The non-resonant background is understood as the difference between the full distribution (black curve) and the DPA unpolarized one (gray curve), the interference among polarizations as the difference between the DPA unpolarized one and the sum of doubly-polarized distributions (magenta curve).

The most relevant variables for polarization measurements are the decay angles of leptons ($\phi_\ell^*, \theta_\ell^*$) in the corresponding weak-boson rest frame. At variance with the inclusive setup, in the presence of lepton cuts a closed analytic formula for $\cos\theta_\ell^*$ distributions is not known, but the distributions for different polarization modes typically maintain visible shape differences, which make $\cos\theta_\ell^*$ variables the best suited ones for polarization discrimination. Note that if polarization vectors are defined in the CM (LAB) frame, the angles of the decay lepton ℓ of a boson V should be computed boosting the ℓ momentum into the V rest frame from the CM (LAB) frame. Such variables are not directly accessible at the LHC, as the W -boson kinematics (and consequently the one of the di-boson system) is only known up to neutrino reconstruction, which can be quite inaccurate in describing some phase-space regions. For the purpose of this work we assume perfect reconstruction of the neutrino momentum.

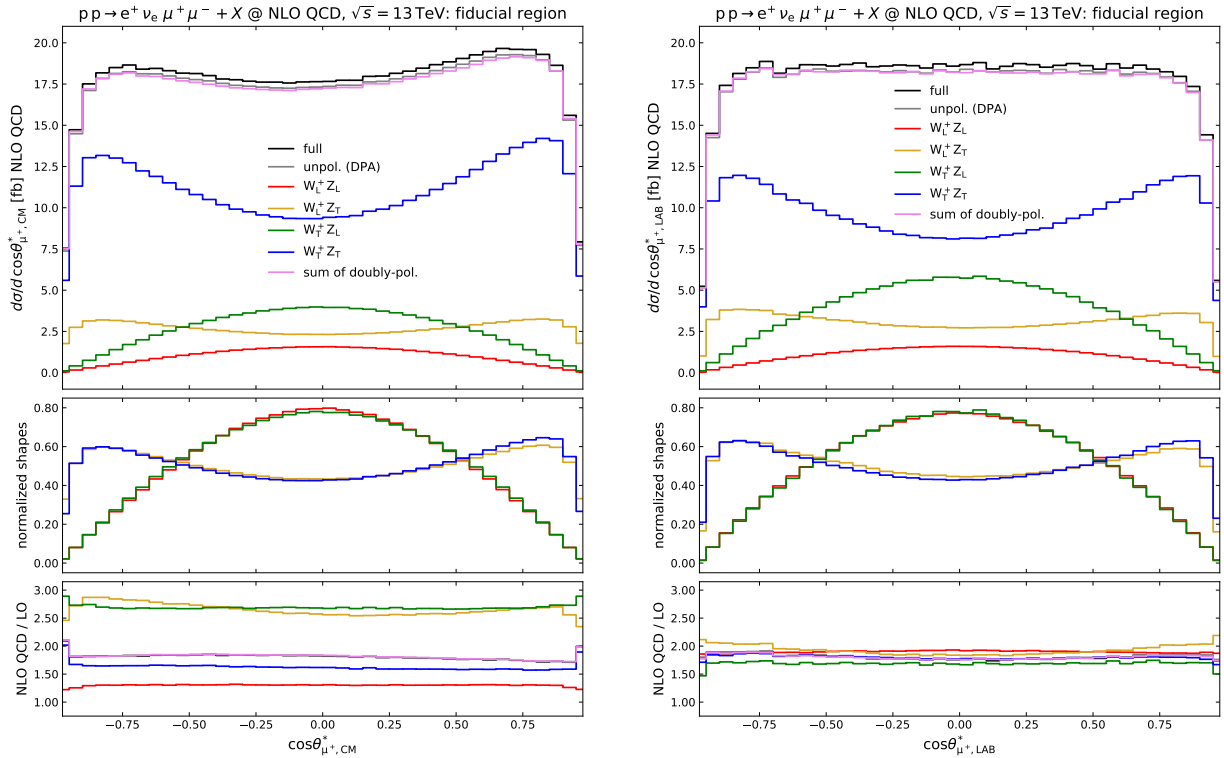


Figure 1: Distributions in $\cos \theta_{\mu^*}^*$ in the fiducial region for polarizations defined in the CM frame (left) and in the LAB frame (right). The antimuon angle in the Z-boson rest frame, $\theta_{\mu^*}^*$, is computed with respect to the Z-boson direction in the CM frame (left) and in the LAB frame (right). Doubly-polarized results are shown. From top down: NLO QCD differential cross-sections, NLO QCD normalized distribution shapes (integral equal to 1), K -factors (NLO QCD / LO).

In Figure 1 we consider the distribution in the antimuon decay angle in the Z-boson rest frame. If polarizations are defined in the LAB frame, this variable is directly observable at the LHC. In the CM case, it is subject to the reconstruction of the di-boson system: we have checked numerically with a neutrino reconstruction technique used in Ref. [4] that this has an almost negligible effect on the shape of $\cos \theta_{\mu^*}^*$ distributions. The K -factors reflect the integrated results. Note that the effect of p_T and η cuts on μ^\pm is to cut down the peaks at $\cos \theta_{\mu^*}^* = \pm 1$ of the transverse distributions (TT, LT), while the LL and TL shapes are almost untouched. While the unpolarized distribution shows an asymmetry in the CM definition, this is washed out when using the LAB definition of the decay angle. The asymmetry in the CM case results from the TT mode, while the distributions are basically symmetric for the other polarization modes. For the LAB definition, on the other hand, an asymmetry develops for the LT mode which is, however, less relevant in view of the much smaller contribution of this mode. Up to the differences in the overall cross sections and the asymmetries, the description of this variable is very similar in the CM and LAB definitions. As the normalized shapes in Figure 1 show, the $\cos \theta_{\mu^*}^*$ variable is only sensitive to the polarization of the Z boson. For a given state of the Z boson, the shape is approximately the same for a longitudinal and a transverse W boson. This means that such a variable should be combined with other discriminating variables to allow for the doubly-polarized extraction via a template-fitting procedure.

The W^+ -boson polarization state is directly related to the $\cos \theta_{e^+}^*$ variable. It is worth stressing that the neutrino reconstruction would affect this variable much more than $\cos \theta_{\mu^*}^*$, since it modifies the kinematics of both the di-boson system (needed for the CM definition) and the W-boson momentum (needed for both definitions). We have checked that using the reconstruction of Ref. [4], the shapes are substantially distorted, leading to a reduced discrimination power among polarization states. Assuming perfect neutrino reconstruction, the resulting $\cos \theta_{e^+}^*$ distributions are shown in Figure 2. The transverse and unpolarized distributions are characterized by a depletion at $\cos \theta_{e^+}^* = -1$, but not at $\cos \theta_{e^+}^* = 1$, since no direct p_T or rapidity constraint is imposed on the neutrino. Analogous situations have been noticed in W^+W^- production [24] and WZ scattering [35]. In both definitions, the shapes for a longitudinal W boson (LL, LT) are made slightly asymmetric by the lepton cuts, but are almost independent of the Z-boson polarization. A different behaviour is found for the two transverse distributions (TL, TT), whose shapes are mildly sensitive to the Z-boson polarization. More interestingly, in the CM definition the TT shape is more peaked at negative values than the TL, while in the LAB one such a difference is reversed and more sizeable. This means that, depending on the Z polarization, there is a different left-right polarization balance of the W boson. The K -factors are roughly equal to those of the integrated cross-sections, up to some deviation in the anti-collinear regime for the CM-frame transverse modes. In both definitions, the K -factors are less flat

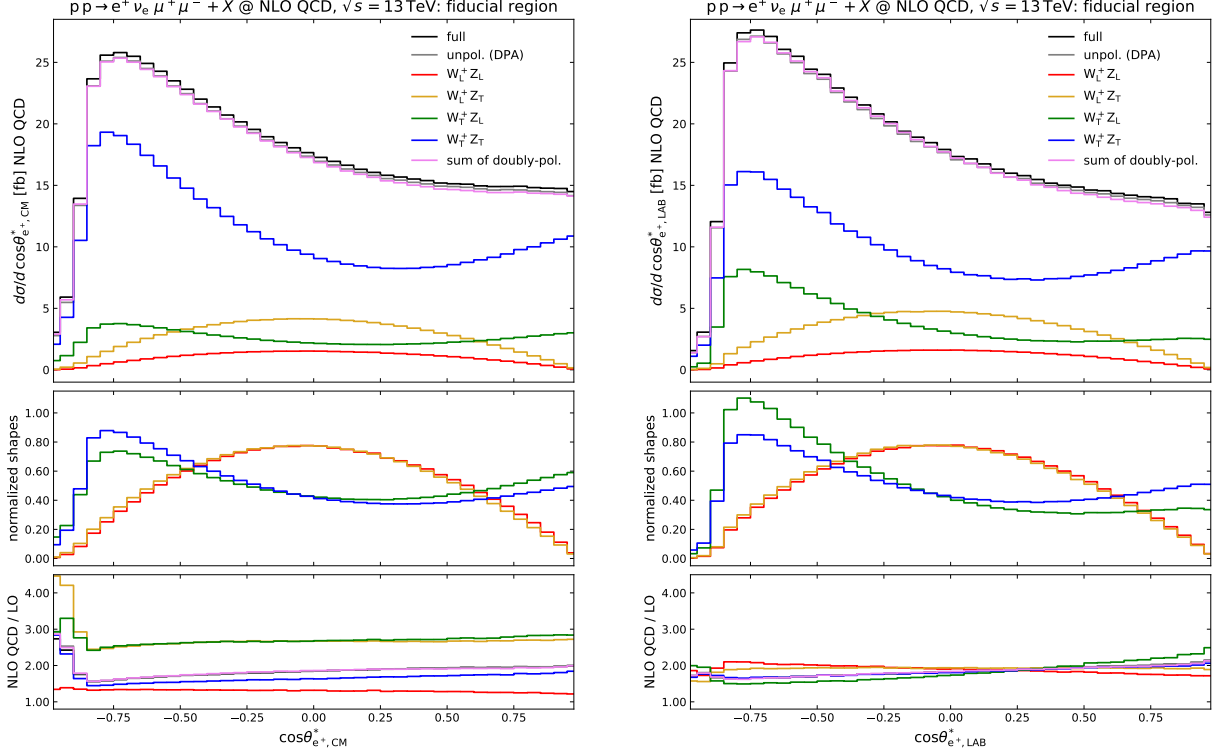


Figure 2: Distributions in $\cos \theta_{e^+}^*$ in the fiducial region for polarizations defined in the CM frame (left) and in the LAB frame (right). The positron angle in the W-boson rest frame, $\theta_{e^+}^*$, is computed with respect to the W-boson direction in the CM frame (left) and in the LAB frame (right). Same structure as Figure 1.

than those observed in $\cos \theta_{\mu^+}^*$ distributions. The different behaviour of $\cos \theta_{e^+}^*$ distributions with respect to the $\cos \theta_{\mu^+}^*$ ones can be traced back to the different nature of the cuts imposed on the W-decay leptons (asymmetric, stronger p_T cut, transverse-mass constraint) and of those imposed on the Z-boson decay products (symmetric, weaker p_T cut, invariant-mass constraint).

A satisfactory fit of LHC data with SM templates can only be achieved with the combination of several kinematic observables which are best suited to discriminate among doubly-polarized signals. We have generated NLO QCD accurate SM templates for many observables. In general, the transverse-momentum distributions (for e^+ , μ^\pm , Z and missing energy) do not show sizeable differences among polarized signals. A mild discrimination power, in particular for the LL mode, is found in the rapidity separation between the positron and the muon, both in the CM and in the LAB definition.

Noticeable differences between the LAB and CM definitions can be seen in the positron-rapidity distributions, which are shown in Figure 3. This variable shows almost negligible interferences and a non-resonant background in line with the integrated result. The relative NLO QCD corrections to the LL signal become maximal near the cut $y_{e^+} = \pm 2.5$ in both definitions, but the size is much larger in the LAB-frame definition than in the CM one. All other polarized signals based on the CM definition have roughly the same differential K-factors, with QCD corrections that are maximal at zero rapidity. Differently from TT and TL, the LT signal in the LAB definition is mostly enhanced by QCD corrections near $y_{e^+} = \pm 2$. In the CM

definition, all polarized signals have a maximum at zero rapidity, though with somewhat different shapes. In particular, the TT signal is flatter than all the other ones. Much more sizeable shape differences characterize the signals in the LAB definition. The TL signal has two maxima around $y_{e^+} = \pm 2$, and a minimum at zero rapidity, where all other doubly-polarized modes have a maximum. The LL, LT, and TT modes have similar normalized shapes, but slightly different peak widths.

The marked difference between the TL and LT distributions in the LAB-frame definition, which is even more evident at LO, can be traced back to the boost that relates the LAB and the CM reference frames. If the polarizations are defined in the CM frame, all polarized rapidity distributions follow similar patterns, as might be expected from the more universal character of this definition. However, due to different PDF densities (the u-quark PDF peaks at larger energies than the \bar{d} -quark one) connecting the CM frame to the LAB frame involves a boost preferentially in the direction of the u quark. Moreover, in the CM frame the W^+ boson is preferably produced in the hemisphere determined by the u-quark direction. As a consequence, the boost to the LAB frame typically accelerates the W^+ boson, while it decelerates the Z boson. Upon inspecting the explicit form of the polarization vectors, it can be seen that a boost that increases the energy changes the polarization vectors only mildly, while a boost that reduces the energy yields more sizeable changes in polarization. In extreme cases the boost results in a very small momentum along the z axis or even reverses this component. Thus, in events with a large y_{W^+} the polarization

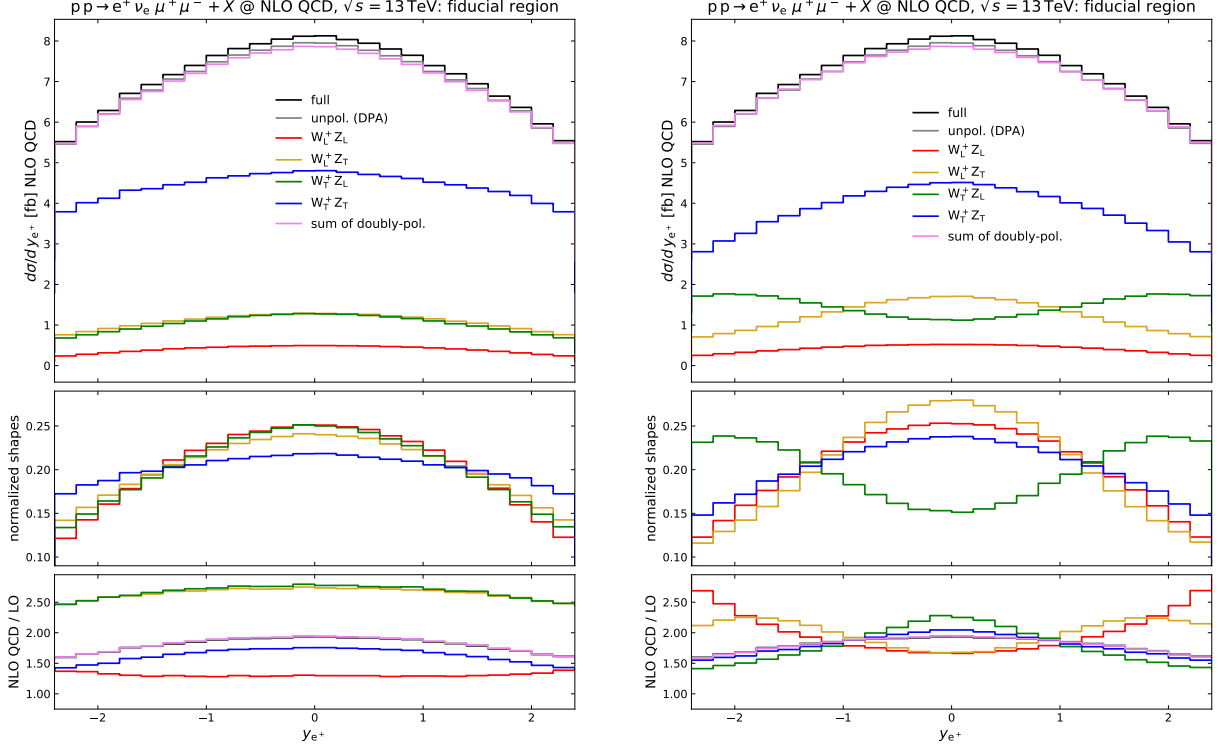


Figure 3: Distributions in the positron rapidity in the fiducial region for polarizations defined in the CM frame (left) and in the LAB frame (right). Same structure as Figure 1.

of the W^+ boson is hardly changed by the boost to the LAB frame, while the one for the Z changes relatively often. On the other hand, in events with a small y_{W^+} the polarization of the W^+ is likely to change, while the one of the Z is pretty stable. Since the W rapidity is correlated to the positron rapidity, this explains the enhancement of the $W_T^+ Z_L$ mode for large y_{e^+} and the enhancement of the $W_L^+ Z_T$ mode for small y_{e^+} via migration from the dominant $W_T^+ Z_T$ mode.

Even though the results for the positron rapidity suggest that investigating polarizations defined in the LAB frame provides more discrimination power than in the CM frame, we stress that the measured quantities are different in the two cases and cannot be related to each other. Thus, two separate analyses for polarizations defined in the CM frame and in the LAB frame are useful.

We have investigated more rapidity observables (for Z , μ^\pm) which feature similar or smaller discrimination power than y_{e^+} .

Another interesting variable accessible at the LHC is the cosine of the angle $\theta_{e^+\mu^-}$ between the positron and the muon, which is presented in Figure 4. In the fiducial region, the two leptons tend to be mostly collinear in the unpolarized case, but different behaviours are found for the polarized modes. The relative QCD corrections are rather flat for the LL signal defined in the CM frame, but increasing with $\cos\theta_{e^+\mu^-}$ for the corresponding signal defined in the LAB frame. The K -factor for the TT mode is monotonically increasing and similar in the two definitions. A similar pattern is found for TL and LT defined in the CM frame, up to the overall shift already commented

at the integrated level. The mixed contributions show decreasing K -factors in the LAB definition. In the CM definition, the normalized TT distribution is almost symmetric, while modes including a longitudinal boson are rather flat for negative values and have a maximum in the collinear regime. Very small shape differences characterize the LL, LT and TL distributions. Only the TT signal can be clearly disentangled. For polarizations defined in the LAB frame, the TT distribution favours anticollinear configurations, while the LL and LT modes show similar behaviours as for the CM definitions. The TL distribution has a peak in the collinear region that is more marked than the one of LL and LT modes. The more sizeable differences among different polarization states in the LAB frame for large $\cos\theta_{e^+\mu^-}$ can again be explained by effects of the boost from the CM frame to the LAB one and its effect on the polarization of the weak bosons. A small angle between positron and muon is correlated to a small angle between the W^+ and the Z boson. This requires the reversal of the z component of one of the vector bosons, mostly of the Z boson, by the boost and thus explains the observed sizeable reshuffling between polarized cross-sections for large $\cos\theta_{e^+\mu^-}$.

In Figure 5 we show the distribution in the azimuthal difference between the positron and the muon. This observable is characterized by negative interferences for $\Delta\phi_{e^+\mu^-} \lesssim \pi/2$ and positive ones for $\Delta\phi_{e^+\mu^-} \gtrsim \pi/2$ in both the CM- and the LAB-frame polarization definitions. Although the interferences are similar in shape to those found in W^+W^- production [24], their size ($\pm 3.5\%$ for $\Delta\phi_{e^+\mu^-} = 0, \pi$) is much smaller than the $\pm 50\%$

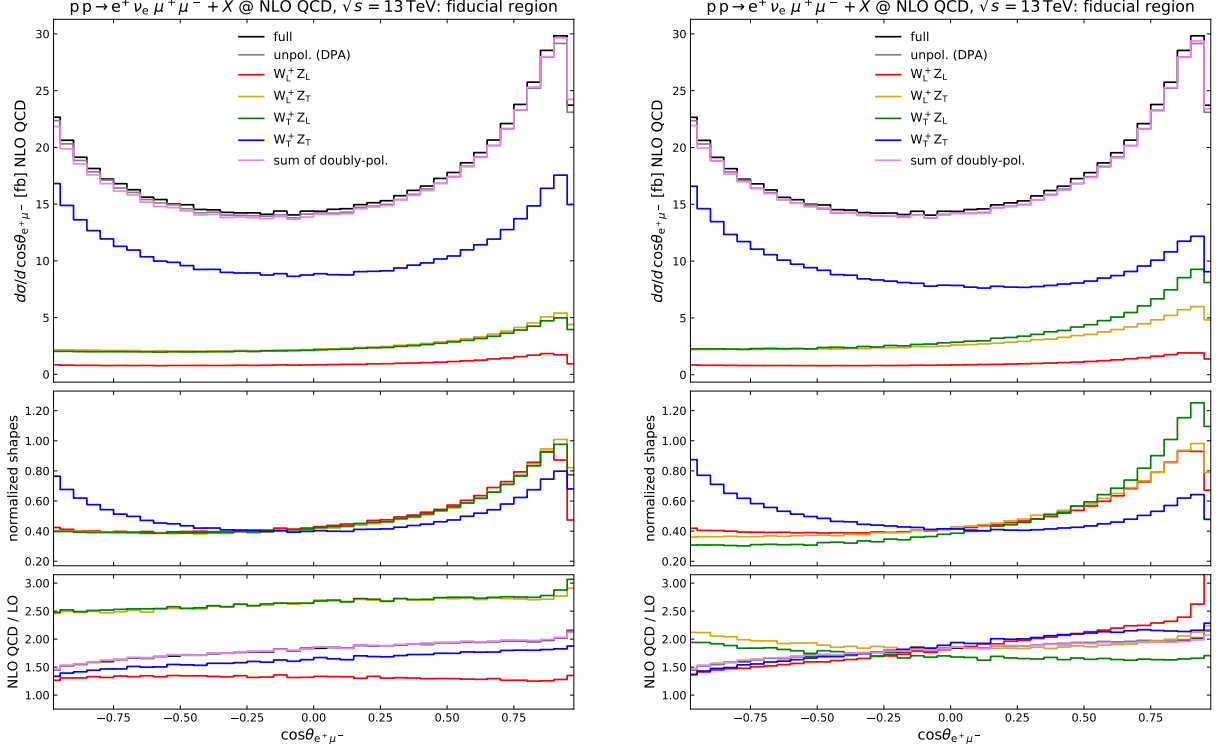


Figure 4: Distributions in the cosine of the angle between the positron and the muon in the fiducial region for polarizations defined in the CM frame (left) and in the LAB frame (right). Same structure as Figure 1.

effect found there. The polarized distributions become maximal at $\Delta\phi_{e^+\mu^-} = \pi$ in both polarization definitions, and all K -factors are decreasing with growing $\Delta\phi_{e^+\mu^-}$. The K -factor of the LL mode is flatter in the CM definition, while the one of the mixed contributions is flatter in the LAB one. All polarization states with at least one transverse boson exhibit roughly the same normalized distribution shape, which is also very similar in the two definitions of polarization vectors. A significantly different shape is found in the LL polarization state both in the LAB and even stronger in the CM definition. This makes this azimuthal separation a good candidate variable to improve the sensitivity to the purely longitudinal cross-section.

As a last comment of this section, we stress that the differential distributions analyzed in this paper do not provide an exhaustive list of physical quantities relevant for the extraction of doubly-polarized signals out of WZ data, but are representative for observables that are best suited for polarization discrimination (in the CM and/or in the LAB definition), and that highlight relevant differences between the two polarization definitions.

4. Conclusions

In this paper we have presented integrated and differential cross-sections for the WZ production at the LHC with both bosons polarized. The results feature NLO QCD accuracy and have been obtained for realistic selection cuts.

The non-resonant background, estimated as the effects missing in the double-pole-approximated calculation, are at the 2%

level for the integrated cross-sections. Slightly larger effects are found in the tails of some distributions, which are, however, out of reach with the statistics of the Run 2 data.

We have investigated polarized signals defining polarization vectors both in the di-boson centre-of-mass (CM) and in the laboratory (LAB) system. In both cases the interferences among different polarization modes are very small (of order 1%). The integrated and differential cross-sections for a given polarization state obtained with the two definitions are rather different, in particular, for the doubly-polarized signals. We have analyzed the impact of NLO QCD corrections, the relative fractions for the various polarization states, and the normalized shapes for several kinematic distributions.

A small number of observables are characterized by a noticeable discrimination power among polarizations. Some of them are more sensitive to polarizations defined in the CM frame, some to those defined in the LAB frame. This suggests that both definitions should be taken into account in the upcoming experimental analyses.

Acknowledgements

We thank Lucia Di Ciaccio, Corinne Goy, Francesco Costanza and Emmanuel Sauvan for useful discussions. The authors are supported by the German Federal Ministry for Education and Research (BMBF) under contract no. 05H18WWCA1.

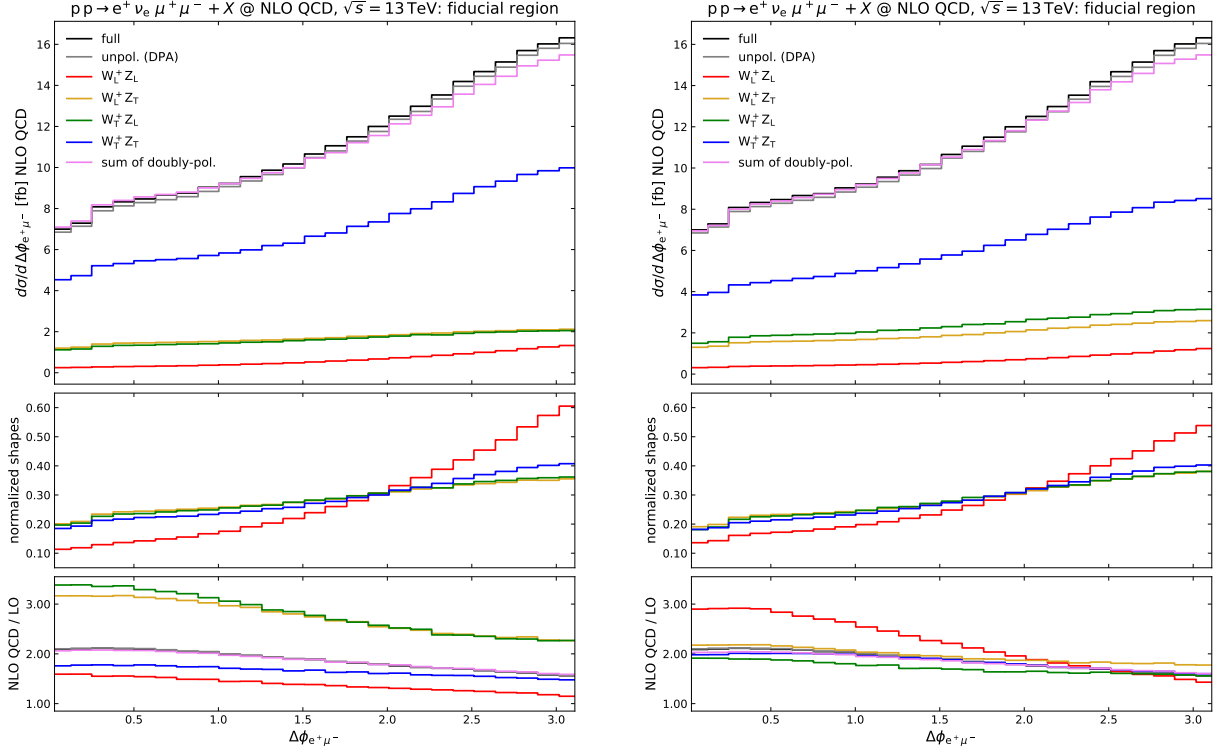


Figure 5: Distributions in the azimuthal difference between the positron and the muon in the fiducial region for polarizations defined in the CM frame (left) and in the LAB frame (right). Same structure as Figure 1.

References

- [1] V. Khachatryan, et al., Measurement of the WZ production cross section in pp collisions at $\sqrt{s} = 13$ TeV, *Phys. Lett. B* 766 (2017) 268–290. [arXiv:1607.06943](#), [doi:10.1016/j.physletb.2017.01.011](#).
- [2] M. Aaboud, et al., Measurement of the $W^\pm Z$ boson pair-production cross section in pp collisions at $\sqrt{s} = 13$ TeV with the ATLAS Detector, *Phys. Lett. B* 762 (2016) 1–22. [arXiv:1606.04017](#), [doi:10.1016/j.physletb.2016.08.052](#).
- [3] A. M. Sirunyan, et al., Measurements of the $pp \rightarrow WZ$ inclusive and differential production cross section and constraints on charged anomalous triple gauge couplings at $\sqrt{s} = 13$ TeV, *JHEP* 04 (2019) 122. [arXiv:1901.03428](#), [doi:10.1007/JHEP04\(2019\)122](#).
- [4] M. Aaboud, et al., Measurement of $W^\pm Z$ production cross sections and gauge boson polarisation in pp collisions at $\sqrt{s} = 13$ TeV with the ATLAS detector, *Eur. Phys. J. C* 79 (6) (2019) 535. [arXiv:1902.05759](#), [doi:10.1140/epjc/s10052-019-7027-6](#).
- [5] J. Ohnemus, An Order α_s calculation of hadronic $W^\pm Z$ production, *Phys. Rev. D* 44 (1991) 3477–3489. [doi:10.1103/PhysRevD.44.3477](#).
- [6] S. Frixione, P. Nason, G. Ridolfi, Strong corrections to W Z production at hadron colliders, *Nucl. Phys. B* 383 (1992) 3–44. [doi:10.1016/0550-3213\(92\)90668-2](#).
- [7] A. Bierweiler, T. Kasprzik, J. H. Kühn, Vector-boson pair production at the LHC to $O(\alpha^3)$ accuracy, *JHEP* 12 (2013) 071. [arXiv:1305.5402](#), [doi:10.1007/JHEP12\(2013\)071](#).
- [8] J. Baglio, L. D. Ninh, M. M. Weber, Massive gauge boson pair production at the LHC: a next-to-leading order story, *Phys. Rev. D* 88 (2013) 113005, [Erratum: *Phys.Rev.D* 94, 099902 (2016)]. [arXiv:1307.4331](#), [doi:10.1103/PhysRevD.94.099902](#).
- [9] B. Biedermann, A. Denner, L. Hofer, Next-to-leading-order electroweak corrections to the production of three charged leptons plus missing energy at the LHC, *JHEP* 10 (2017) 043. [arXiv:1708.06938](#), [doi:10.1007/JHEP10\(2017\)043](#).
- [10] M. Grazzini, S. Kallweit, D. Rathlev, M. Wiesemann, $W^\pm Z$ production at hadron colliders in NNLO QCD, *Phys. Lett. B* 761 (2016) 179–183. [arXiv:1604.08576](#), [doi:10.1016/j.physletb.2016.08.017](#).
- [11] M. Grazzini, S. Kallweit, D. Rathlev, M. Wiesemann, $W^\pm Z$ production at the LHC: fiducial cross sections and distributions in NNLO QCD, *JHEP* 05 (2017) 139. [arXiv:1703.09065](#), [doi:10.1007/JHEP05\(2017\)139](#).
- [12] M. Grazzini, S. Kallweit, J. M. Lindert, S. Pozzorini, M. Wiesemann, NNLO QCD + NLO EW with Matrix+OpenLoops: precise predictions for vector-boson pair production, *JHEP* 02 (2020) 087. [arXiv:1912.00068](#), [doi:10.1007/JHEP02\(2020\)087](#).
- [13] T. Becher, M. Hager, Event-Based Transverse Momentum Resummation, *Eur. Phys. J. C* 79 (8) (2019) 665. [arXiv:1904.08325](#), [doi:10.1140/epjc/s10052-019-7136-2](#).
- [14] P. Nason, G. Zanderighi, W^+W^- , WZ and ZZ production in the POWHEG-BOX-V2, *Eur. Phys. J. C* 74 (1) (2014) 2702. [arXiv:1311.1365](#), [doi:10.1140/epjc/s10052-013-2702-5](#).
- [15] M. Chiesa, C. Oleari, E. Re, NLO QCD+NLO EW corrections to diboson production matched to parton shower, *Eur. Phys. J. C* 80 (9) (2020) 849. [arXiv:2005.12146](#), [doi:10.1140/epjc/s10052-020-8419-3](#).
- [16] U. Baur, T. Han, J. Ohnemus, WZ production at hadron colliders: Effects of nonstandard WWZ couplings and QCD corrections, *Phys. Rev. D* 51 (1995) 3381–3407. [arXiv:hep-ph/9410266](#), [doi:10.1103/PhysRevD.51.3381](#).
- [17] R. Franceschini, G. Panico, A. Pomarol, F. Riva, A. Wulzer, Electroweak Precision Tests in High-Energy Diboson Processes, *JHEP* 02 (2018) 111. [arXiv:1712.01310](#), [doi:10.1007/JHEP02\(2018\)111](#).
- [18] M. Chiesa, A. Denner, J.-N. Lang, Anomalous triple-gauge-boson interactions in vector-boson pair production with RECOLA2, *Eur. Phys. J. C* 78 (6) (2018) 467. [arXiv:1804.01477](#), [doi:10.1140/epjc/s10052-018-5949-z](#).
- [19] J. Baglio, S. Dawson, S. Homiller, QCD corrections in Standard Model EFT fits to WZ and WW production, *Phys. Rev. D* 100 (11) (2019) 113010. [arXiv:1909.11576](#), [doi:10.1103/PhysRevD.100.113010](#).
- [20] W. J. Stirling, E. Vryonidou, Electroweak gauge boson polarisation at the LHC, *JHEP* 07 (2012) 124. [arXiv:1204.6427](#), [doi:10.1007/JHEP07\(2012\)124](#).
- [21] J. Baglio, N. Le Duc, Fiducial polarization observables in hadronic WZ

- production: A next-to-leading order QCD+EW study, JHEP 04 (2019) 065. [arXiv:1810.11034](#), [doi:10.1007/JHEP04\(2019\)065](#).
- [22] J. Baglio, L. D. Ninh, Polarization observables in WZ production at the 13 TeV LHC: Inclusive case, *Commun. Phys.* 30 (1) (2020) 35–47. [arXiv:1910.13746](#), [doi:10.15625/0868-3166/30/1/14461](#).
- [23] D. Buarque Franzosi, O. Mattelaer, R. Ruiz, S. Shil, Automated predictions from polarized matrix elements, JHEP 04 (2020) 082. [arXiv:1912.01725](#), [doi:10.1007/JHEP04\(2020\)082](#).
- [24] A. Denner, G. Pelliccioli, Polarized electroweak bosons in W^+W^- production at the LHC including NLO QCD effects, JHEP 09 (2020) 164. [arXiv:2006.14867](#), [doi:10.1007/JHEP09\(2020\)164](#).
- [25] A. M. Sirunyan, et al., Measurements of production cross sections of polarized same-sign W boson pairs in association with two jets in proton-proton collisions at $\sqrt{s} = 13$ TeV, *Phys. Lett. B* 812 (2021) 136018. [arXiv:2009.09429](#), [doi:10.1016/j.physletb.2020.136018](#).
- [26] A. Ballestrero, E. Maina, G. Pelliccioli, Different polarization definitions in same-sign WW scattering at the LHC, *Phys. Lett. B* 811 (2020) 135856. [arXiv:2007.07133](#), [doi:10.1016/j.physletb.2020.135856](#).
- [27] Z. Bern, et al., Left-Handed W Bosons at the LHC, *Phys. Rev. D* 84 (2011) 034008. [arXiv:1103.5445](#), [doi:10.1103/PhysRevD.84.034008](#).
- [28] A. Aeppli, F. Cuypers, G. J. van Oldenborgh, $O(\Gamma)$ corrections to W pair production in e^+e^- and $\gamma\gamma$ collisions, *Phys. Lett. B* 314 (1993) 413–420. [arXiv:hep-ph/9303236](#), [doi:10.1016/0370-2693\(93\)91259-P](#).
- [29] A. Aeppli, G. J. van Oldenborgh, D. Wyler, Unstable particles in one loop calculations, *Nucl. Phys. B* 428 (1994) 126–146. [arXiv:hep-ph/9312212](#), [doi:10.1016/0550-3213\(94\)90195-3](#).
- [30] W. Beenakker, F. A. Berends, A. P. Chapovsky, Radiative corrections to pair production of unstable particles: results for $e^+e^- \rightarrow 4$ fermions, *Nucl. Phys. B* 548 (1999) 3–59. [arXiv:hep-ph/9811481](#), [doi:10.1016/S0550-3213\(99\)00110-8](#).
- [31] A. Denner, S. Dittmaier, M. Roth, D. Wackerth, Electroweak radiative corrections to $e^+e^- \rightarrow WW \rightarrow 4$ fermions in double-pole approximation: The RACOONWW approach, *Nucl. Phys. B* 587 (2000) 67–117. [arXiv:hep-ph/0006307](#), [doi:10.1016/S0550-3213\(00\)00511-3](#).
- [32] M. Billoni, et al., Next-to-leading order electroweak corrections to $pp \rightarrow W^+W^- \rightarrow 4$ leptons at the LHC in double-pole approximation, JHEP 12 (2013) 043. [arXiv:1310.1564](#), [doi:10.1007/JHEP12\(2013\)043](#).
- [33] B. Biedermann, M. Billoni, A. Denner, S. Dittmaier, L. Hofer, B. Jäger, L. Salfelder, Next-to-leading-order electroweak corrections to $pp \rightarrow W^+W^- \rightarrow 4$ leptons at the LHC, JHEP 06 (2016) 065. [arXiv:1605.03419](#), [doi:10.1007/JHEP06\(2016\)065](#).
- [34] A. Ballestrero, E. Maina, G. Pelliccioli, W boson polarization in vector boson scattering at the LHC, JHEP 03 (2018) 170. [arXiv:1710.09339](#), [doi:10.1007/JHEP03\(2018\)170](#).
- [35] A. Ballestrero, E. Maina, G. Pelliccioli, Polarized vector boson scattering in the fully leptonic WZ and ZZ channels at the LHC, JHEP 09 (2019) 087. [arXiv:1907.04722](#), [doi:10.1007/JHEP09\(2019\)087](#).
- [36] S. Actis, A. Denner, L. Hofer, A. Scharf, S. Uccirati, Recursive generation of one-loop amplitudes in the Standard Model, JHEP 04 (2013) 037. [arXiv:1211.6316](#), [doi:10.1007/JHEP04\(2013\)037](#).
- [37] S. Actis, A. Denner, L. Hofer, J.-N. Lang, A. Scharf, S. Uccirati, RECOLA: REcursive Computation of One-Loop Amplitudes, *Comput. Phys. Commun.* 214 (2017) 140–173. [arXiv:1605.01090](#), [doi:10.1016/j.cpc.2017.01.004](#).
- [38] A. Denner, S. Dittmaier, L. Hofer, COLLIER - A fortran-library for one-loop integrals, *PoS LL2014* (2014) 071. [arXiv:1407.0087](#).
- [39] A. Denner, S. Dittmaier, L. Hofer, COLLIER: a fortran-based Complex One-Loop Library in Extended Regularizations, *Comput. Phys. Commun.* 212 (2017) 220–238. [arXiv:1604.06792](#), [doi:10.1016/j.cpc.2016.10.013](#).
- [40] S. Catani, M. Seymour, A general algorithm for calculating jet cross-sections in NLO QCD, *Nucl. Phys. B* 485 (1997) 291–419, [Erratum: *Nucl. Phys. B* 510 (1998) 503–504]. [arXiv:hep-ph/9605323](#), [doi:10.1016/S0550-3213\(96\)00589-5](#).
- [41] A. Buckley, J. Ferrando, S. Lloyd, K. Nordström, B. Page, M. Rüfenacht, M. Schönherr, G. Watt, LHAPDF6: parton density access in the LHC precision era, *Eur. Phys. J. C* 75 (2015) 132. [arXiv:1412.7420](#), [doi:10.1140/epjc/s10052-015-3318-8](#).
- [42] M. Tanabashi, et al., Review of Particle Physics, *Phys. Rev. D* 98 (3) (2018) 030001. [doi:10.1103/PhysRevD.98.030001](#).
- [43] D. Bardin, A. Leike, T. Riemann, M. Sachwitz, Energy-dependent width effects in e^+e^- annihilation near the Z-boson pole, *Phys. Lett. B* 206 (1988) 539–542. [doi:10.1016/0370-2693\(88\)91627-9](#).
- [44] A. Denner, S. Dittmaier, M. Roth, L. Wieders, Electroweak corrections to charged-current $e^+e^- \rightarrow 4$ fermion processes: Technical details and further results, *Nucl. Phys. B* 724 (2005) 247–294, [Erratum: *Nucl. Phys. B* 854 (2012) 504]. [arXiv:hep-ph/0505042](#), [doi:10.1016/j.nuclphysb.2011.09.001](#).
- [45] A. Denner, S. Dittmaier, The complex-mass scheme for perturbative calculations with unstable particles, *Nucl. Phys. Proc. Suppl.* 160 (2006) 22–26. [arXiv:hep-ph/0605312](#), [doi:10.1016/j.nuclphysbps.2006.09.025](#).
- [46] R. D. Ball, et al., Parton distributions from high-precision collider data, *Eur. Phys. J. C* 77 (10) (2017) 663. [arXiv:1706.00428](#), [doi:10.1140/epjc/s10052-017-5199-5](#).
- [47] U. Baur, T. Han, J. Ohnemus, Amplitude zeros in $W^\pm Z$ production, *Phys. Rev. Lett.* 72 (1994) 3941–3944. [arXiv:hep-ph/9403248](#), [doi:10.1103/PhysRevLett.72.3941](#).
- [48] A. Belyaev, D. Ross, What does the CMS measurement of W-polarization tell us about the underlying theory of the coupling of W-bosons to matter?, JHEP 08 (2013) 120. [arXiv:1303.3297](#), [doi:10.1007/JHEP08\(2013\)120](#).